scientific reports

OPEN

Real-time monitoring of bioelectrical impedance for minimizing tissue carbonization in microwave ablation of porcine liver

Xiao Zhang[1,3], Wei Wei[1,3], Lu Qian[2,3], Liuye Yao[2,3], Xiaofei Jin[2,3✉], Lidong Xing[1,3✉] & Zhiyu Qian[2,3]

The charring tissue generated by the high temperature during microwave ablation can affect the therapeutic effect, such as limiting the volume of the coagulation zone and causing rejection. This paper aimed to prevent tissue carbonization while delivering an appropriate thermal dose for effective ablations by employing a treatment protocol with real-time bioelectrical impedance monitoring. Firstly, the current field response under different microwave ablation statuses is analyzed based on finite element simulation. Next, the change of impedance measured by the electrodes is correlated with the physical state of the ablated tissue, and a microwave ablation carbonization control protocol based on real-time electrical impedance monitoring was established. The finite element simulation results show that the dielectric properties of biological tissues changed dynamically during the ablation process. Finally, the relative change rule of the electrical impedance magnitude of the *ex vivo* porcine liver throughout the entire MWA process and the reduction of the central zone carbonization were obtained by the MWA experiment. Charring tissue was eliminated without water cooling at 40 W and significantly reduced at 50 W and 60 W. The carbonization during MWA can be reduced according to the changes in tissue electrical impedance to optimize microwave thermal ablation efficacy.

Microwave ablation (MWA), known for its broad ablation range, wide indications, and minimal heat deposition effect, has been widely used in treating solid tumors such as liver tumors[1–4]. In MWA, direct energy deposition in the ablation zone leads to elevated temperatures in surrounding tissues. The ablated zone is prone to carbonization, resulting in dehydrated carbonized tissue. The "carbonized" zone is close to the antenna axis, at higher temperatures, the tissue appears charred, highly desiccated, and black. A more peripheral zone of complete thermal denaturation of proteins is known as "white coagulation"[5]. Previous studies have shown that in the MWA of some organs, such as the spleen[6], the crushing and avulsion of charring tissues in the course of needle withdrawal can cause bleeding. Carbonized tissue impedes heat dispersion, causing the ablation zone to adopt an ellipsoidal shape rather than spherical[7]. The carbonization phenomenon may also induce both regional and systemic inflammatory responses and other unwanted side effects[8–10]. Precise control of microwave output for ablating tumors effectively while avoiding tissue carbonization is important for clinical MWA.

Researchers propose minimally invasive thermometry to prevent carbonization by inserting single-point or multipoint thermometry needles for local temperature measurement[11,12]. Ultrasound-based thermometry remains insufficient for deep temperature field distribution measurement in liver tissue[13]. Additionally, the degree of tissue inactivation, as per the kinetic properties of thermal injury in biological tissues, necessitates evaluation based on temperature and exposure duration, indicating that assessing tissue ablation efficacy solely based on temperature is insufficient[14,15]. Some researchers have suggested the cyclic pulse microwave output ablation mode[16–19], which partly lowers the maximum temperature in the central ablation zone, reducing carbonization occurrence. Still, achieving a consistent, less carbonization effect under different parameters is impossible. Various water-cooled antennas have also been developed to prevent overhigh temperatures and

[1]Department of Electrical Engineering, College of Automation Engineering, Nanjing University of Aeronautics and Astronautics, Nanjing 211106, China. [2]Department of Biomedical Engineering, College of Automation Engineering, Nanjing University of Aeronautics and Astronautics, Nanjing 211106, China. [3]Key Laboratory of Multi-modal Brain-Computer Precision Drive, Industry and Information Technology Ministry, Nanjing University of Aeronautics and Astronautics, Nanjing 211106, China. ✉email: jinxiaofei@nuaa.edu.cn; xiaoz20172019@163.com

decrease the probability of carbonizing[20]. However, the water flow will carry away a lot of heat while reducing carbonization, resulting in a limited volume of coagulation zone.

Recently, the dielectric properties of tissues have garnered widespread attention among researchers. Yero et al. established a correlation between the dielectric properties of ablated tissues, the duration of action, and thermal damage during heating[15]. Amini et al. concluded that changes in the pathological and physiological characteristics of biological tissues, which also alter their dielectric properties, can be assessed via bioimpedance measurements[21]. Leung et al. photolithographically engraved electrodes and wires for electrical impedance detection on the surface of an ablation probe, facilitating impedance measurements during laser ablation, ensured precise local control of impedance measurements during laser-induced heat treatment of *ex vivo* porcine liver tissues[22]. In irreversible electroporation ablation, Zhao et al. assessed changes in liver tissue impedance spectra induced by pulsed electric fields and composite pulsed percutaneous puncture ablation of porcine liver tissues[23]. The results indicated that the overall ablation effect could be indirectly inferred from the impedance spectra. While these studies did not directly investigate carbonization effects, they provided valuable insights into carbonization control protocols.

This paper aims to investigate the variation of electrical impedance in liver tissue during MWA and develop an effective method for reducing carbonization based on electrical impedance. In this paper, an electrical impedance monitoring system during MWA was established to measure the changes of electrical impedance during microwave ablation of porcine liver, and a method to reduce carbonization based on monitoring the magnitude of electrical impedance change was proposed. The effects of two ablation protocols, electrical impedance control microwave delivery and continuous microwave delivery, on the charring tissue formation and ablation efficiency of *ex vivo* porcine liver were evaluated.

Material and method
Simulation of electrical characteristics of tissues during MWA
Finite element simulations were conducted using COMSOL Multiphysics software (Version 6.0, Stockholm, Sweden, https://cn.comsol.com/support). Figure 1a shows a two-dimensional axisymmetric physical model of
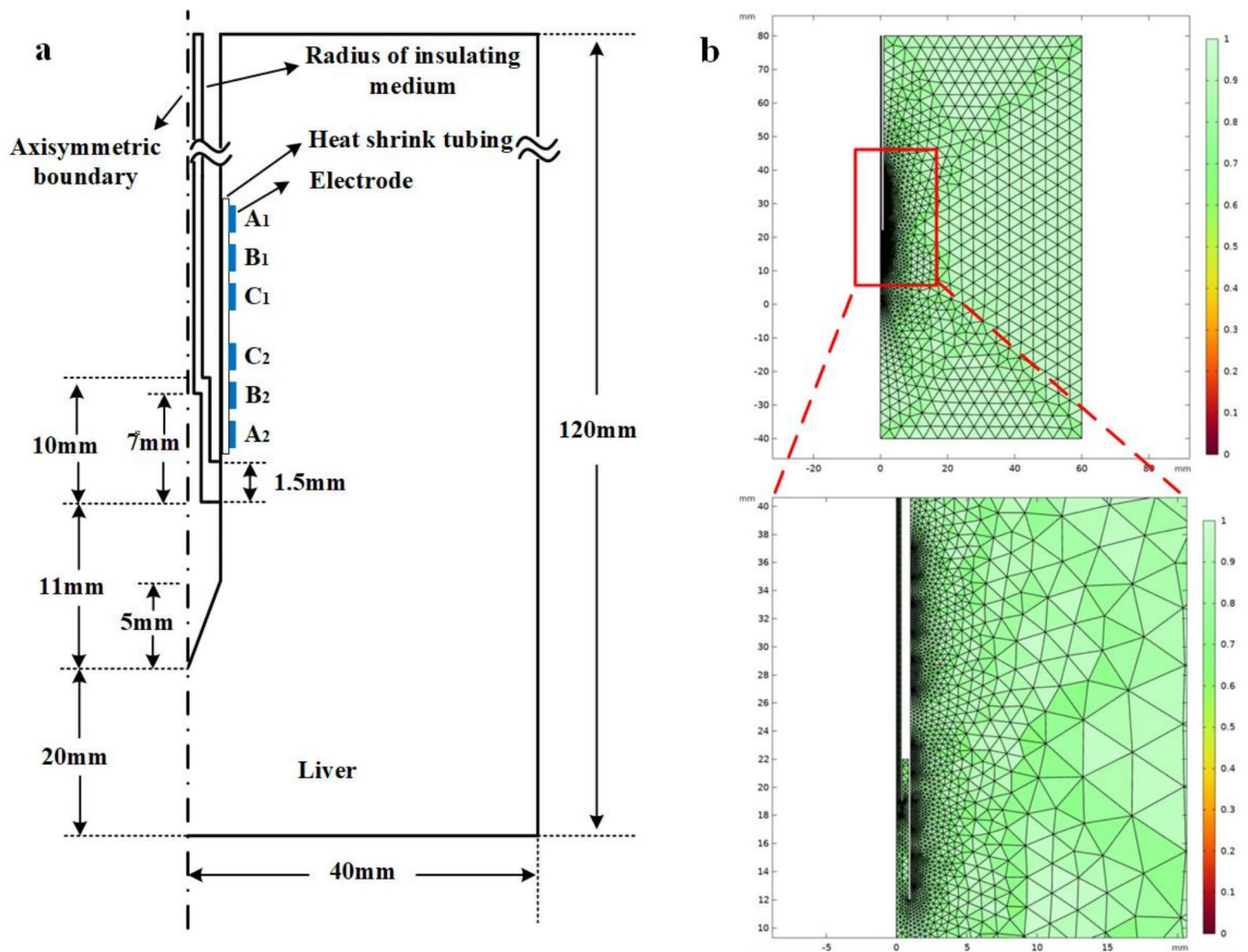
Fig. 1. (**a**) Geometric model of simulated MWA of *ex vivo* porcine liver. (**b**) Mass map of finite element mesh profiles.

the ablation probe and the *ex vivo* porcine liver, incorporating electrodes into the existing microwave ablation model[19]. The geometric model of the microwave antenna and porcine liver tissue is reduced to an axisymmetric structure to reduce the calculation time. Table 1 presents the structural parameters of the probe and the electrode parameters utilized in the simulation model, with liver tissue designated as the thermal ablation zone (120 mm, 60 mm). The model is discretized into grid cells using the finite element method, as shown in Fig. 1b. As the current density around the electrode is higher than in other zones, augmenting the mesh density in its vicinity enhances simulation accuracy. Ultimately, a finite element mesh comprising 8082 triangular cells, 1755 edge cells, and 46 vertex cells is generated, with an average cell mass of 0.8381 and a minimum cell mass of 0.1885.

The construction of *ex vivo* porcine liver MWA simulation model includes the following steps:

Step 1: The electromagnetic wave propagation equation and Penne's heat transfer equation were coupled to obtain the simulated temperature field of microwave ablation. The electromagnetic wave propagation equation is expressed as:

$$\nabla^2 E - \mu\sigma\frac{\partial E}{\partial t} - \mu\varepsilon\frac{\partial^2 E}{\partial t^2} = 0 \tag{1}$$

where μ is the magnetic permeability, σ is the conductivity, ε is the relative dielectric permittivity, and E is the electric field strength.

The Pennes heat transfer equation is expressed as:

$$\rho C\frac{\partial T}{\partial t} = \nabla(k\nabla T) + Q_{ext} \tag{2}$$

where ρ is the density, C is the specific heat capacity, k is the thermal conductivity, and Q_{ext} is the external heat source. Q_{ext} is microwave energy absorbed by biological tissues, and a process of converting microwave energy into thermal energy can be expressed as:

$$Q_{ext} = \frac{\sigma|E|^2}{2} \tag{3}$$

Set the simulation parameters. It mainly includes the dielectric property parameters, the biological heat conduction parameters of liver tissue, and the material parameters of the MWA antenna. The thermal conductivity (k), density (ρ), relative dielectric permittivity (ε), conductivity (σ), and specific heat capacity (C) of the liver are as follows[24]:

$$k(T) = \begin{cases} 0.512; & 293.15\ K \leq T \leq 363.15\ K \\ 0.2027\ T - 17.933; & 363.15\ K < T \leq 373.15\ K \\ 0.0053\ T^2 - 1.727\ T + 64.681; & 373.15\ K < T \leq 386.15\ K \\ 0.21; & 386.15\ K < T \leq 473.15\ K \end{cases} \tag{4}$$

$$\rho(T) = \begin{cases} 1050; & 293.15\ K \leq T \leq 373.15\ K \\ 294; & 373.15\ K < T \leq 473.15\ K \end{cases} \tag{5}$$

$$\varepsilon(T) = 48.391\left\{1 - \frac{1}{1 + \exp[0.0764(82.271 - T + 273.15)]}\right\}$$
$$+ 1;\ 293.15\ K \leq T \leq 473.15\ K \tag{6}$$

$$\sigma(T) = 2.713\left\{1 - \frac{1}{1 + \exp[0.0697(85.375 - T + 273.15)]}\right\};$$
$$293.15\ K \leq T \leq 473.15\ K \tag{7}$$

Parameter	Value	Unit
Radius of antenna	0.95	mm
Radius of insulating medium (top)	0.4	mm
Radius of insulating medium (middle)	0.55	mm
Radius of insulating medium (bottom)	0.95	mm
Radius of the inner conductor	0.15	mm
Insulating medium opening	1.5	mm
Piercing head length	11	mm
Number of electrodes	6	N/A
Thickness of electrode	0.2	mm
Width of electrode	2	mm

Table 1. Structural and electrode parameters of the probe[19].

$$C(T) = \begin{cases} 3600; \ 273.15 \ K \leq T \leq 373.15 \ K \\ 327800; \ 373.15 \ K < T \leq 378.15 \ K \\ 2103; \ 378.15 \ K < T \leq 473.15 \ K \end{cases} \quad (8)$$

The dielectric property parameters and tissue heat conduction parameters used in the simulation model are shown in Table 2[19,24].

Step 2: Set the current field control equations under impedance measurement. This results in minimal conduction current and negligible magnetic field generation due to the low frequency, which allows for considering a quasi-static electric field without compromising engineering calculation accuracy. When the current with angular frequency ω is applied, the mathematical equation is expressed as:

$$\begin{cases} \nabla \cdot ((\sigma + j\omega\varepsilon)\nabla\varphi) = 0 \\ \delta = \sigma + j\omega\varepsilon \end{cases} \quad (9)$$

where j denotes the vector sign, δ is the complex conductivity, and φ is the potential.

The Dirichlet boundary condition is defined as:

$$\varphi(x,y) = f(x,y) \quad (x,y) \in \partial\Omega \quad (10)$$

The Neumann boundary condition is defined as:

$$-\delta(x,y)\frac{\partial\varphi(x,y)}{\partial n} = J(x,y) \quad (x,y) \in \partial\Omega \quad (11)$$

where $\partial\Omega$ is the boundary of the field, f is the Dirichlet boundary condition function, and n is the direction of the normal outside the boundary.

The articulation condition of the sub-interface within the field is expressed as:

$$\delta_1 \frac{\partial\varphi_1}{\partial n} = \delta_2 \frac{\partial\varphi_2}{\partial n} \quad (12)$$

Setting up the current field control equations, including the boundary conditions, calculated the potential value. The impedance value was also derived since the current was used as an excitation source.

Step 3: Set the microwave frequency (2450 MHz), ablation power, and ablation time to start the MWA simulation. Due to the probe's limited spatial coverage and the minimal impact of electrode size on the current field compared to electrode spacing was kept at a constant length. Electrodes A_1–A_2 were spaced 26 mm apart, electrodes B_1–B_2 were spaced 18 mm apart, and electrodes C_1–C_2 were spaced 10 mm apart. The excitation electrode frequency was set to 20 kHz, and the current magnitude was 0.5 mA in this paper[25].

For enhanced visualization of differences, the magnitude of measured impedances under different excitation electrodes is shown in Fig. 2. For example, in Fig. 2, when A_1–A_2 are set as the excitation electrodes, the measured impedances are obtained for electrodes B_1–B_2 and C_1–C_2, respectively. The simulation results also showed that the impedance measurements at the moments of 120 s, 150 s, and 180 s were different and showed an increasing trend with time, i.e., the electrical properties of different ablation zone states influence the potential distribution. Additionally, the differences in impedance changes between different electrode pairs may be due to the different positions in which they are located.

	Parameter	Symbol	Value	Unit
Liver	Thermal conductivity	k_{liver}	Formula (4)	W·m⁻¹·K⁻¹
	Density	ρ_{liver}	Formula (5)	kg·m⁻³
	Relative dielectric constant	ε_{liver}	Formula (6)	1
	Conductivity	σ_{liver}	Formula (7)	S·m⁻¹
	Specific heat capacity	C_{liver}	Formula (8)	J·kg⁻¹·K⁻¹
PTFE	Relative dielectric constant	ε_{PTFE}	2	1
	Conductivity	σ_{PTFE}	0	S·m⁻¹
	Density	ρ_{PTFE}	2200	kg·m⁻³
	Thermal conductivity	k_{PTFE}	0.24	W·m⁻¹·K⁻¹
	Specific heat capacity	C_{PTFE}	1050	J·kg⁻¹·K⁻¹
Copper	Density	ρ_{copper}	8960	kg·m⁻³
	Thermal conductivity	k_{copper}	400	W·m⁻¹·K⁻¹
	Specific heat capacity	C_{copper}	385	J·kg⁻¹·K⁻¹

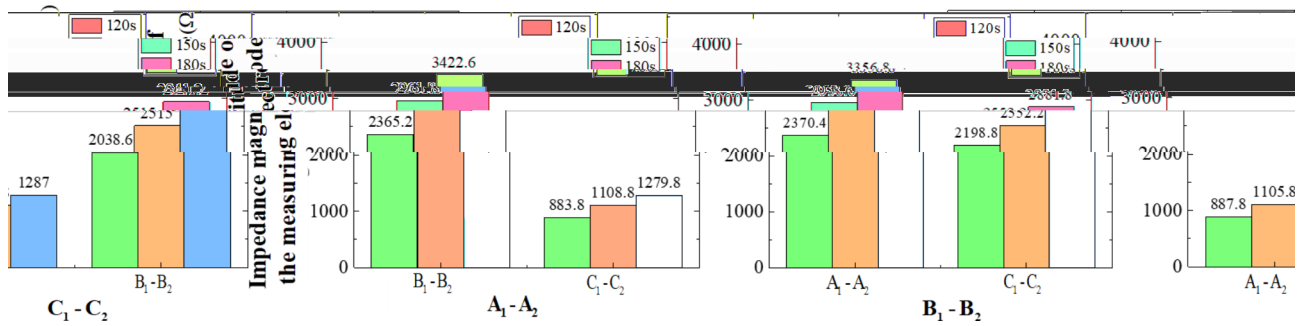**Table 2.** Parameters used in the simulation model.

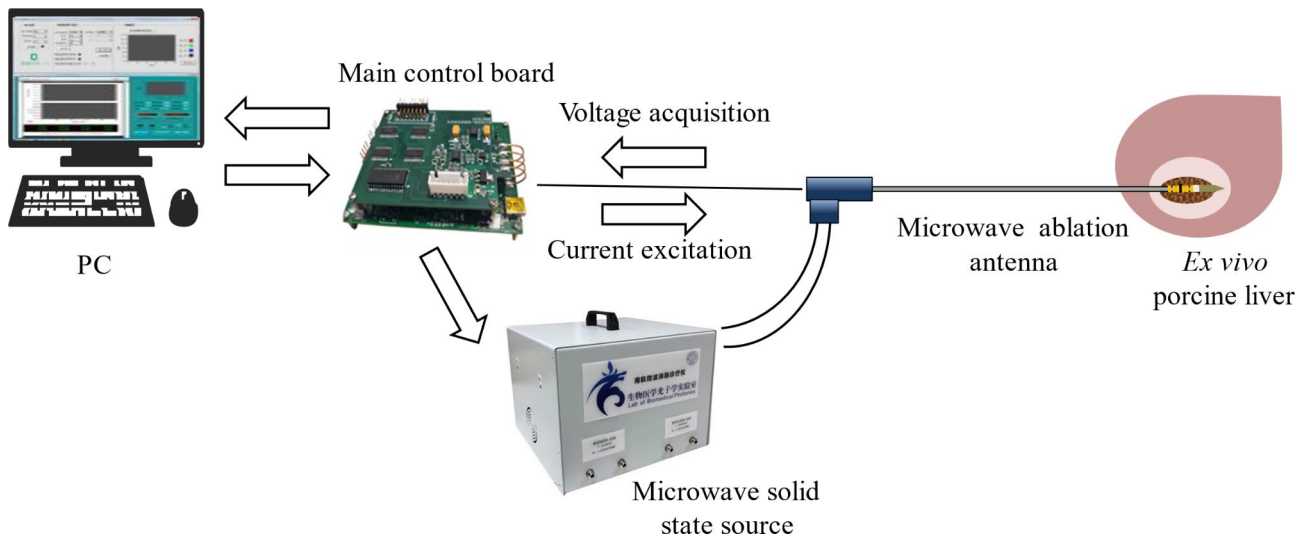**Fig. 2**. Impedance magnitudes with various excitation electrodes.

Fig. 3. The system for measuring bioelectrical impedance during MWA.

## System for measuring bioelectrical impedance during MWA

As shown in Fig. 3, the MWA system is composed of a microwave solid state source (Bada Microwave Technology Co., Ltd., Hangzhou, China), a microwave ablation antenna (Kangyou Medical Instruments, Nanjing, China), a personal computer (PC), and an in-house built main control board. The microwave solid state source can output microwave power in the range of 1–100 W at a frequency of 2450 MHz. The microwave ablation antenna (KY-2450-B1) is 13 cm long and 1.9 mm in diameter. We improved the microwave ablation antenna by adding a temperature sensor and six electrodes at the front of the antenna, distributed around the energy radiation point of the microwave ablation antenna. The temperature sensor is a packaged NTC (Negative Temperature Coefficient) thermistor with a resistance value of 10 kΩ, insulated and waterproof, which can measure temperature changes between 0 and 200 ℃. The PC can adjust the microwave output parameters by communicating with the main control board. Similarly, the main control board transmits the collected temperature and electrical impedance data to the PC for recording.

The capacitive component prevalent in impedance detection was considered to enhance the accuracy assessment of the proposed electrical impedance measurement device. This paper introduces two equivalent circuit models as loads[26], as shown in Fig. 4. The accuracy and precision of the measurement results are evaluated using the relative standard deviation (RSD) and signal-to-noise ratio (SNR) as follows:

$$\text{RSD} = \frac{std(\sum_m v_{i,j})}{mean(\sum_m v_{i,j})} \times 100\% \tag{13}$$

$$\text{SNR} = 10\log_{10}\left(\frac{\sum_m v_{i,j}^2}{\sum_m \left(v_{i,j} - \bar{v}_{i,j}\right)^2}\right) \tag{14}$$

where $v_{i,j}$ denotes the voltage value acquired on the jth pair of electrodes when the ith pair of electrodes is excited, and m denotes the number of acquisition frames ($m = 50$). $\bar{v}_{i,j}$ denotes the average value of the repetitively acquired voltage of the corresponding channel.
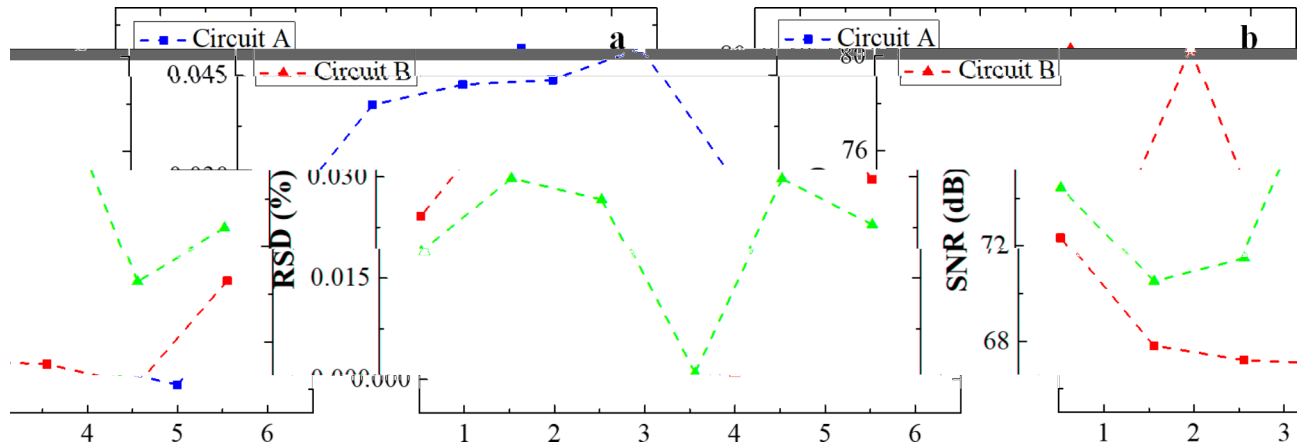
Fig. 4. (**a**) Measurement results of RSD. (**b**) Measurement results of SNR.

The average RSD of the measurement results below 0.04% and an average SNR of 70 dB or higher are good enough for impedance measurements, as shown in Fig. 4a and b. So, the hardware provides good acquisition accuracy and reliable impedance detection.

Electrical impedance measurement during MWA

As shown in Fig. 5a, the structural section of the bioelectrical impedance probe was devised in this study. Six electrodes (blue) were added near the insulating medium sleeve of the microwave ablation antenna. Initially, a transparent heat-shrinkable tube layer was applied to the rear end of the insulating medium sleeve. Subsequently, metal-copper electrodes were wound onto the heat-shrinkable tube's surface, enabling the setup of excitation and measurement electrodes in six configurations (A_1A_2–B_1B_2, A_1A_2–C_1C_2, B_1B_2–A_1A_2, B_1B_2–C_1C_2, C_1C_2–A_1A_2, C_1C_2–B_1B_2). Next, the metal electrodes were connected to the bioelectrical impedance measurement circuit board.

The current path traversed the ablated lesion zone, enabling precise characterization of local tissue status by measuring impedance changes. Typically, electrical impedance testing utilizes a four-electrode system to mitigate the contact impedance effects observed in a two-electrode system[27,28]. As shown in Fig. 5a, each can serve as excitation or measurement electrodes during a measurement cycle. Figure 5b shows the current injection at electrode A and subsequent voltage measurement at electrodes B and C in sequence. Similarly, current injection at B or C electrodes and voltage measurement at other electrodes are shown in Fig. 5c and d, allowing the collection of six groups of voltage data. The excitation electrode injected low-frequency current, while the measurement electrode gauged the response voltage, enabling the calculation of impedance change magnitude. Tissue status in the ablation zone was determined based on impedance change magnitude, guiding decisions to minimize carbonization. To mitigate the high-frequency electromagnetic field's influence on the impedance measurement induced by microwaves, the antenna and electrode lines were mutually exclusive on the switch, and on/off periods were alternated. Impedance measurement occurred post-microwave ablation cessation, as shown in the measurement time sequence in Fig. 5e.

Ex vivo porcine liver impedance measurement experiments during MWA

Fresh *ex vivo* porcine liver was obtained from the local slaughterhouse and used the same day. The experiment was carried out at a room temperature of 25 ℃. Before ablation, the microwave power was set to 40 W, 50 W, and 60 W, respectively, and the cumulative effective ablation duration was 360 s. The water-cooling function of the microwave ablation antenna was not used in the experiment. An initial collection of electrical impedance magnitude preceded ablation. Intermittent pausing for 1 s per every 10 s of ablation aimed to simulate continuous mode effects closely, with impedance magnitude recorded during these pauses. Chapters 1 to 6 were also assigned to different excitation and measurement electrode configurations. Each ablation mode (continuous group and impedance group) involved in this article has been repeated four times ($n = 4$ for each condition) for a total of 24 groups of experiments to ensure the reliability and repeatability of the results. The final data were averaged. To minimize discrepancies arising from liver variability and probe placement, a variable representing the relative change in impedance magnitude pre- and post-ablation, the relative change magnitude of electrical impedance, was used as an index to determine the occurrence of carbonization. Available representing the relative change in impedance magnitude pre-ablation and post-ablation Z_{diff} is defined as:

$$Z_{diff} = \frac{Z'_{real} - Z_{real}}{Z_{real}} \tag{15}$$

where Z'_{real} is the electrical impedance magnitude at each time point after ablation, and Z_{real} is the electrical impedance magnitude before ablation.
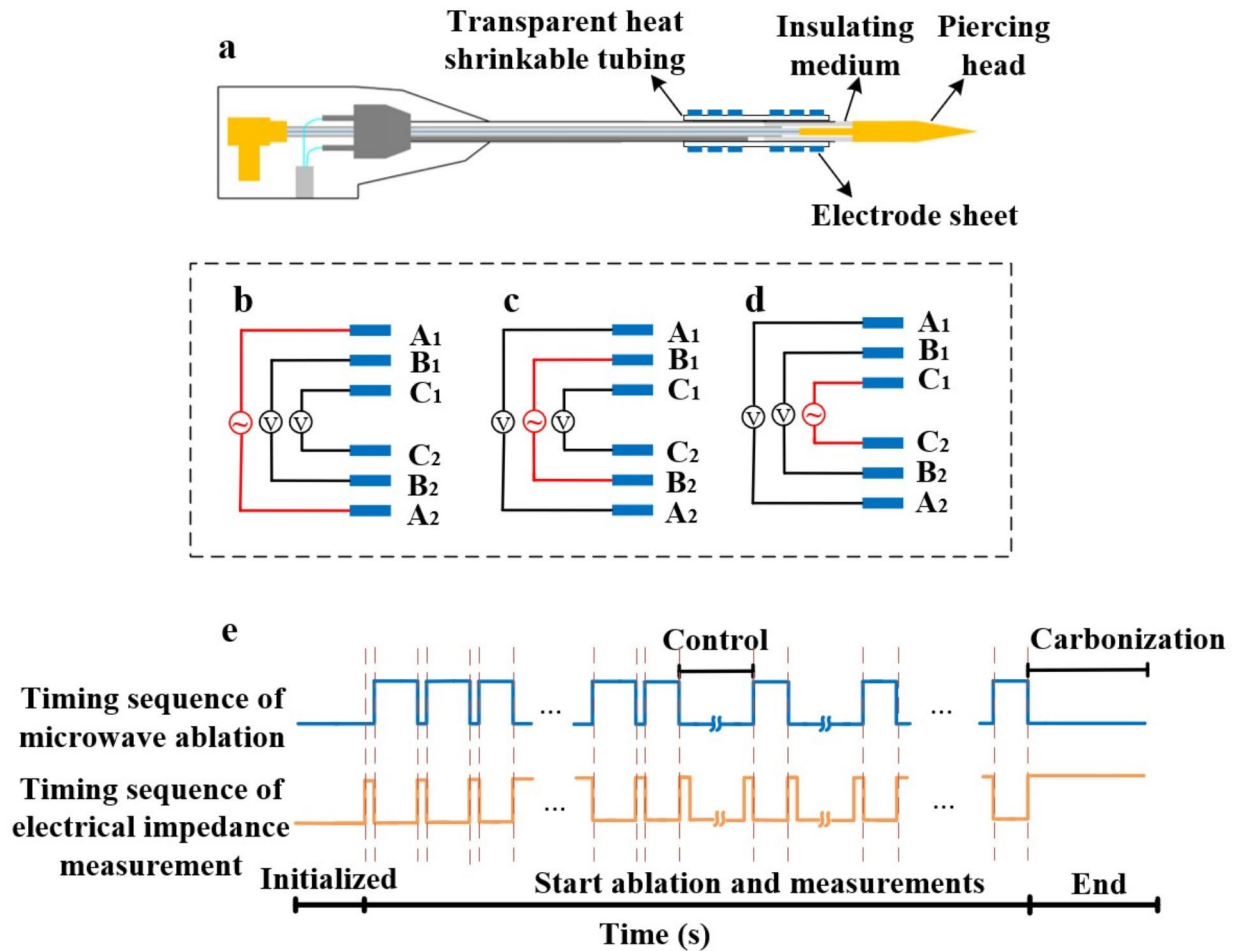
Fig. 5. Profile of the ablation probe featuring electrical impedance measurement and current injection method. (**a**) Probe profile. (**b**) First current injection. (**c**) Second current injection. (**d**) Third current injection. (**e**) Timing sequence of microwave ablation and electrical impedance measurement.

Results
Changes in electrical impedance of porcine liver during MWA under 40 W

Figure 6a and f shows the temporal variation of the average electrical impedance magnitude and temperature of six measurement experiments with continuous ablation of the *ex vivo* porcine liver for 360 s at a microwave power of 40 W. The trend in each channel indicated primarily two notable increases in electrical impedance magnitude. During the pre-ablation period, the electrical impedance magnitude initially rises, peaks around 60 ℃, and then declines while the temperature ascends steadily. In the mid-ablation stage, the electrical impedance magnitude rapidly increases after briefly stabilizing at its nadir, while the temperature stabilizes at around 90% of its peak. Towards the ablation's conclusion, the electrical impedance magnitude surges to higher resistance levels while the temperature nearly stabilizes at its peak. After pausing the ablation, the electrical impedance magnitude and temperature rapidly decrease from their peak values. The trend in electrical impedance magnitude exhibits resemblances to findings in the literature[29–31]. Additionally, variations in electrical impedance magnitude and temperatures among liver tissue in each experimental group stemmed from discrepancies in the *ex vivo* porcine liver and the diverse placements of electrical impedance probes. Nonetheless, the majority of experiments progressed through the four ablations as mentioned above stages.

Ablation results in the *ex vivo* porcine liver of MWA with electrical impedance control under 40 W

To minimize carbonization in the ablation zone, preventing the electrical impedance magnitude from reaching its peak during the process was crucial. The control group was set up, and a 40 W microwave continuously ablated the porcine liver for 360 s. In the experimental group, ablation was initiated at 40 W. The microwave output was halted upon the rapid increase in electrical impedance magnitude and resumed when it returned to a low value until the cumulative ablating time reached 360 s.

Correlating the results with the ablation effect based on a single pair of electrodes was challenging. Therefore, it was imperative to consider the impedance magnitude from all channels. In this study, we aggregate the relative
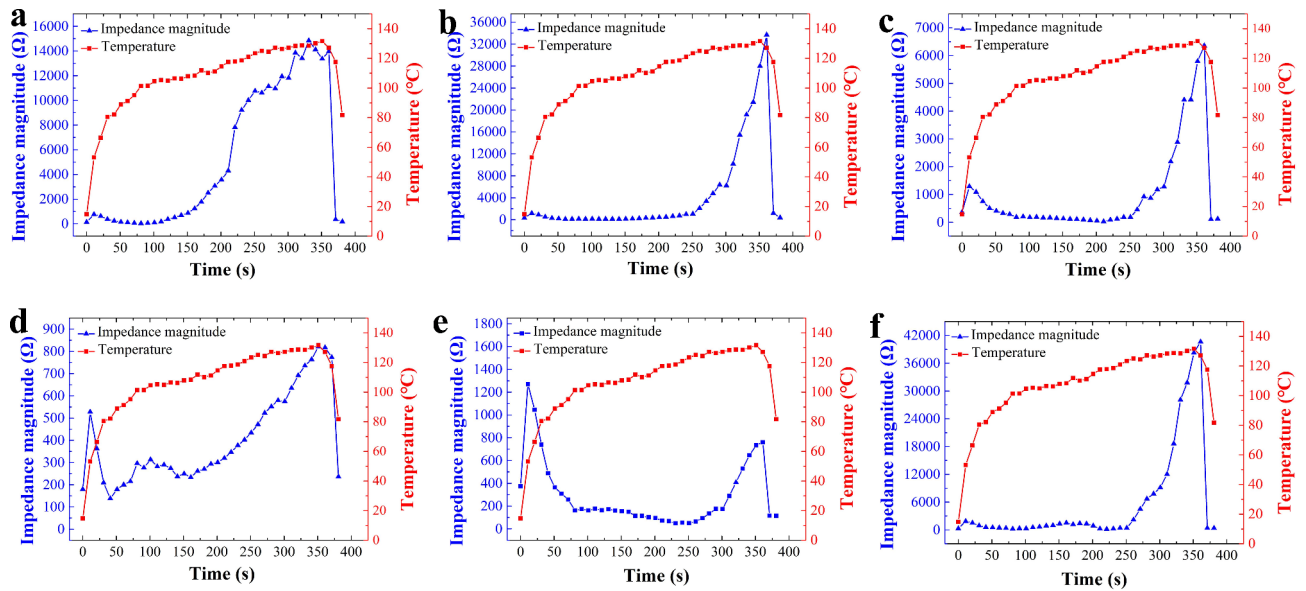
Fig. 6. Trend of electrical impedance magnitude versus temperature over time for 6 channels. (**a**) Channel (1), (**b**) channel (2), (**c**) channel (3), (**d**) channel (4), (**e**) channel (5), (**f**) channel 6.

changes in impedance magnitude-center from all channels, as shown in Fig. 7a. The tissue electrical impedance change magnitude and temperature changes under electrical impedance control during ablation are shown in Fig. 7b. The microwave source is deactivated at 161 s, 241 s, 301 s, 351 s, 431 s, and 481 s, respectively, to ensure the relative change in electrical impedance magnitude stay below 20, which is used as a reference threshold. After each deactivation of the microwave source, the electrical impedance change magnitude exhibits a declining trend, followed by a rapid increase upon reactivation. The coagulation zone measures 45 mm in length and 23 mm in width, with a total ablation time of 511 s. Before employing this method, Fig. 7c shows the experimental outcomes of thermal ablation on *ex vivo* porcine liver, revealing a significant presence of blackened, charred tissue in the central zone. As shown in Fig. 7d, the results from the control group utilizing electrical impedance change magnitude indicate minimal to no presence of charred tissue in the central zone. Hence, the electrical impedance detection method effectively prevented carbonization within the central zone.

Ablation results in the *ex vivo* porcine liver of MWA with electrical impedance control under different powers

As shown in Fig. 8amb, when the relative change in electrical impedance magnitude exceeds 45 (50 W) and 60 (60 W), the microwave source is deactivated, resulting in total ablation times of 671 s and 791 s, respectively. The thresholds for the relative magnitude of change in electrical impedance are different for each power, mainly due to the measurement intervals being fixed at 10 s, and the reference thresholds (20) are easily exceeded in the higher power modes. Figure 8c,d show the effects at 50 W and 60 W power settings before electrical impedance control, demonstrating successful ablation under varying conditions. As shown in Table 3, the carbonization zone's mean maximum length and width are 24 mm and 6.25 mm (50 W, 360 s). For the same duration, the carbonization zone's mean maximum length and width under 60 W are 31 mm and 6.5 mm, respectively. Figure 8e,f show the effect of post-electrical impedance control. Increased microwave energy delivery at 60 W results in larger coagulation zones observed in the *ex vivo* porcine liver and a notable variation in charred tissue formation.

Table 3 also provides the coagulation and carbonization zone dimensions of *ex vivo* porcine liver tissue treated with MWA at power levels of 50 W and 60 W after impedance control, with a cumulative microwave output time set to 360 s. Changes in electrical impedance magnitude typically result in a reduced extent of carbonization compared to pre-electrical impedance control. Notably, due to the higher output power of 60 W, operations became more frequent and progressively more challenging than those at 40 W and 50 W. The coagulation zone's mean long and short diameters are 44.25 mm and 31.25 mm (50 W, 360 s). For the same duration, the coagulation zone's mean long and short diameters under 60 W are 50.5 mm and 32.25 mm, respectively. At 50 W power and an adequate accumulation time of 360 s, minimal charred tissue is observed in the central zone, and the mean maximum length and width of the carbonization zone under 50 W are 14.25 mm and 4 mm. With power at 60 W and an adequate accumulation time of 360 s, the carbonized zone's maximum length and width are reduced to 16.5 mm and 4.5 mm.

Discussion

Analyzing the dynamic changes in electrical magnitude at each MWA stage can enhance carbonization research optimization. Alterations within the ablation zone during MWA correlate with the tissue's physical condition[30]. The notable rise in impedance change magnitude during the pre-melting stage stems from decreased conductivity
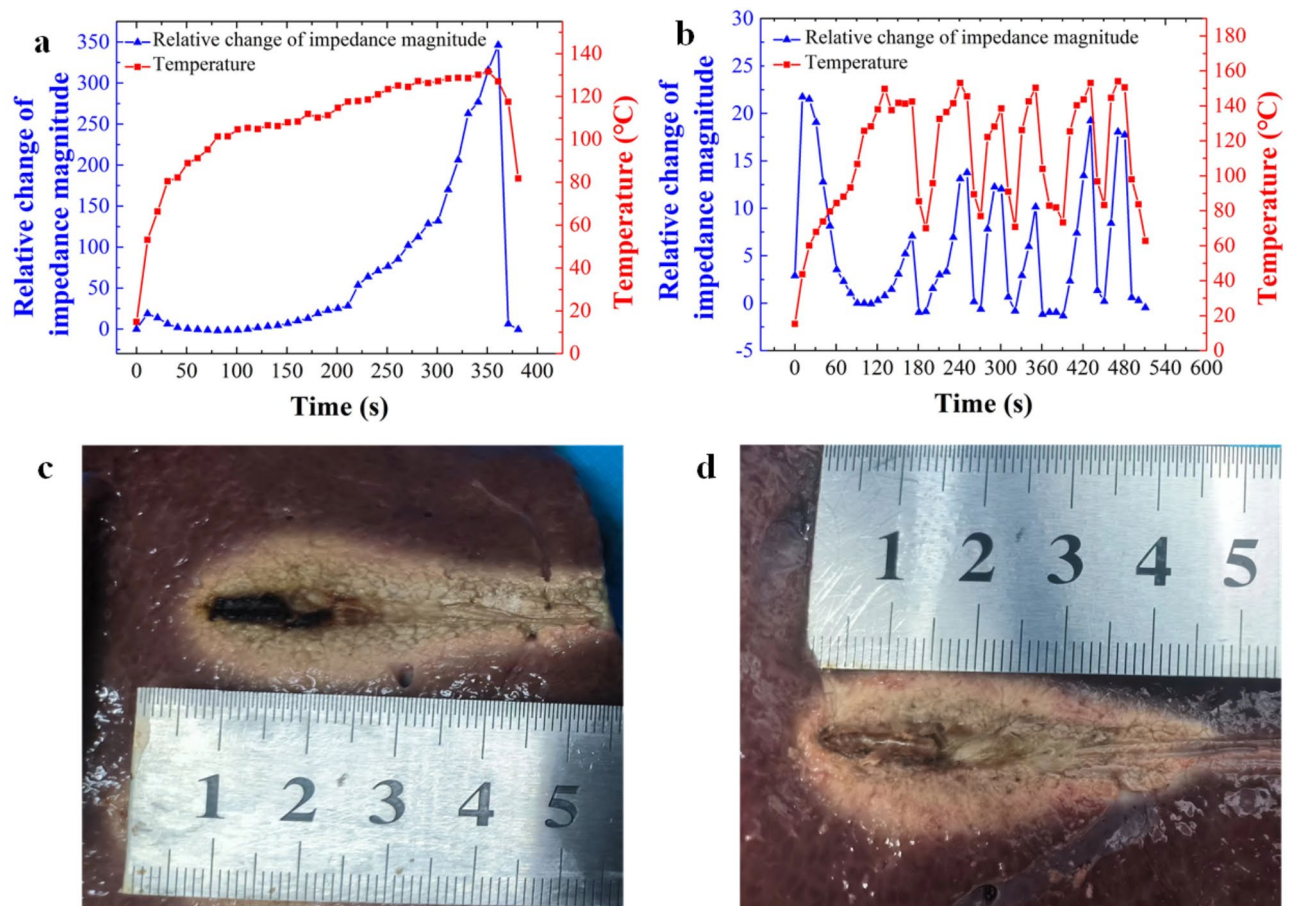
Fig. 7. Trends of electrical impedance change magnitude and temperature during MWA. (**a**) Superimposed results of relative changes in electrical impedance magnitude from channels 1 to 6. (**b**) Results of relative changes in electrical impedance magnitude from channels 1 to 6 after electrical impedance control. (**c**) Actual ablation effect before electrical impedance control. (**d**) Actual ablation effect after electrical impedance control.

induced by rapid warming and dehydration. Subsequently, MWA induces liver tissue cell membrane rupture, facilitating a new pathway for electric current flow. This rupture leads to an outflow of conductive ions from intracellular fluid, augmenting electrical conductivity and reducing impedance. Furthermore, the temperature corresponding to the impedance inflection point precisely reached 60 ℃, as shown in Fig. 6a-f, consistent with prior studies indicating irreversible cellular damage and protein coagulation upon tissue heating to 60 ℃[32–34]. In the mid-ablation stage, the magnitude of the electrical impedance change rapidly increased. Due to widespread cell death, the tissue gradually becomes extremely dry, vaporized, or even carbonized over time, with the zone progressively expanding, the darker the color, and the more severe the carbonization. By the end of ablation, the electrical impedance change magnitude reaches a high value, indicating a significant carbonized zone, as shown in Fig. 7c. Subsequently, post-ablation, peripheral tissue fluid continues to infiltrate the desiccated MWA tissue zone, leading to increased conductivity in this zone and a decrease in impedance.

In this paper, by observing the relative amount of change in the electrical impedance magnitude in real-time and turning on or off the microwave output in time during the period when the electrical impedance change magnitude rises rapidly in the middle of the ablation, the reduction of the carbonized zone is finally achieved, and the ablation effect is shown in Figs. 7d and 8e and f.

High temperature is considered the primary cause of tissue carbonization, prompting the need for temperature control in MWA procedures to prevent carbonization[7,35,36]. Jin et al. identified 130 ℃ as the critical temperature for porcine liver carbonization[19]. However, at 101 s, the temperature in Fig. 7b has reached 130 ℃, yet the tissue remains still not carbonized, and the impedance magnitude has just reached its nadir. Carbonization in MWA necessitates elevated temperatures and prolonged thermal exposure, consistent with the Arrhenius theory of thermal damage[37]. Relying solely on the temperature is unreliable. The local electrical impedance can be a more accurate judge of carbonization than the local temperature.

Advantages of reducing carbonization based on tissue electrical impedance

Compared with the conventional continuous ablation method, although the periodic intermittent pulsed microwave output effectively reduces the carbonization, it also has the disadvantages of a long total ablation time and difficulty achieving non-carbonization[19]. Moreover, the duty cycle of the pulse protocol ablation mode
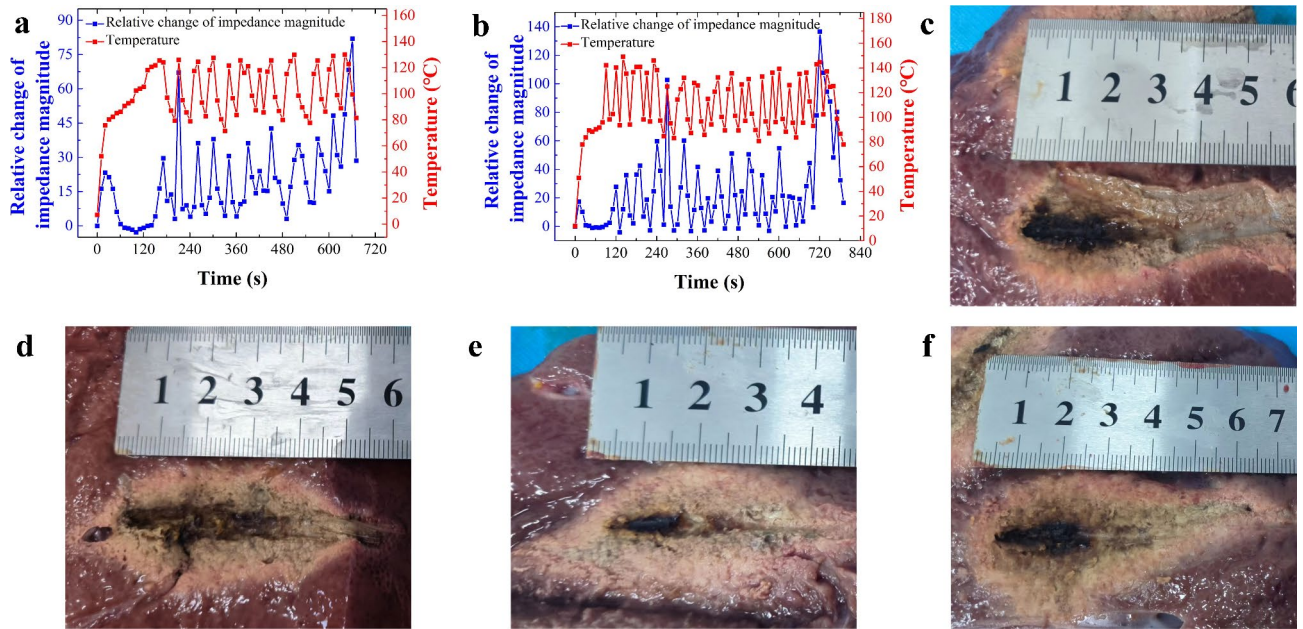
Fig. 8. Trends of electrical impedance change magnitude and temperature during MWA. (**a**) Superimposed results of relative changes in electrical impedance magnitude from channels 1 to 6 after electrical impedance control (50 W, 360 s). (**b**) Superimposed results of relative changes in electrical impedance magnitude from channels 1 to 6 after electrical impedance control (60 W, 360 s). (**c**) Actual ablation effect before electrical impedance control (50 W, 360 s). (**d**) Actual ablation effect before electrical impedance control (60 W, 360 s). (**e**) Actual ablation effect after electrical impedance control (50 W, 360 s). (**f**) Actual ablation effect after electrical impedance control (60 W, 360 s).

Power	Output mode	Group	L_1 (mm)	S_1 (mm)	L_2 (mm)	W_2 (mm)	ML_1 (mm)	MS_1 (mm)	Mean axial ratio	ML_2 (mm)	MW_2 (mm)
50 W	Continuous output	1	45	26	24	6	45	25.5	0.567	24	6.25
		2	46	26	25	7					
		3	44	25	24	6					
		4	45	25	23	6					
	electrical impedance control	1	45	32	15	4	44.25	31.25	0.706	14.25	4
		2	44	32	15	5					
		3	44	30	12	3					
		4	44	31	15	4					
60 W	Continuous output	1	50	31	31	6	50.25	31.75	0.632	31	6.5
		2	52	33	32	7					
		3	52	32	30	6					
		4	51	31	31	7					
	electrical impedance control	1	50	33	17	4	50.5	32.25	0.639	16.5	4.5
		2	51	32	16	5					
		3	51	32	16	5					
		4	50	32	17	4					

Table 3. Dimensions of coagulation zone and carbonization zone in the *ex vivo* porcine liver tissues after various MWA treatments when the cumulative time of microwave output is set to 360 s ($n = 4$ for each condition). L_1: Long diameter of coagulation zone; S_1: Short diameter of coagulation zone; L_2: Maximum length of carbonization zone; W_2: Maximum width of carbonization zone; ML_1: Mean long diameter of coagulation zone; MS_1: Mean short diameter of coagulation zone; ML_2: Mean maximum length of carbonization zone; MW_2: Mean maximum width of carbonization zone.

is not set according to the parameters characterizing carbonization. While water-cooled antennas can reduce carbonization, they also remove most of the heat, limit the volume of the coagulation zone, and increase the cost of the ablation equipment.

In contrast, the method proposed in this paper can accurately detect impedance changes during the MWA, achieve the double beneficial effect of reducing carbonization, and reduce operation time under 40 W, 50 W, and 60 W with no-water cooling. The maximum length and width of the carbonization zone can be significantly reduced. The reduction of carbonization also leads to an increase in the axial ratio of the coagulation zone. Compared with continuous ablation, the maximum length of the liver carbonization zone under the electrical impedance-controlled microwave output protocol was reduced by 40.63% (50–360 s) and 46.77% (60–360 s), respectively.

Limitation of the study

A limitation of this study was that the *in vivo* ablation verification needed to be performed. In this study, the design of the simulation model and actual ablation were performed based on the *ex vivo* porcine liver. The characteristics of *ex vivo* porcine liver tissue are similar to those of the human liver[38]. The most significant difference between *ex vivo* animal tissue experiments and *in vivo* experiments is that there is a rich blood supply in living animal tissues. However, to analyze the carbonization results under different microwave output ablation modes, the experiment often needs to be repeated many times, and the *in vivo* tissue experiment is difficult to carry out on a large scale, so the *ex vivo* tissue experiment is still essential.

The blood perfusion rate and its variation with temperature are influenced by individual differences and other factors. We use the average value reported in the literature for simulation[39], that is when the temperature is less than 333.15 K, the blood perfusion rate is 0.016 s^{-1}. In addition, considering the effect of thermal injury on blood flow, it can be simplified that the blood perfusion rate of tissues above 333.15 K is 0. Through our simulation results at 40 W, it is found that blood perfusion primarily affects the ablation zone by reducing the relative changes in electrical impedance magnitude, as shown in Fig. 9. Compared with the case of no blood perfusion, the relative change in the magnitude of electrical impedance due to the presence of blood perfusion
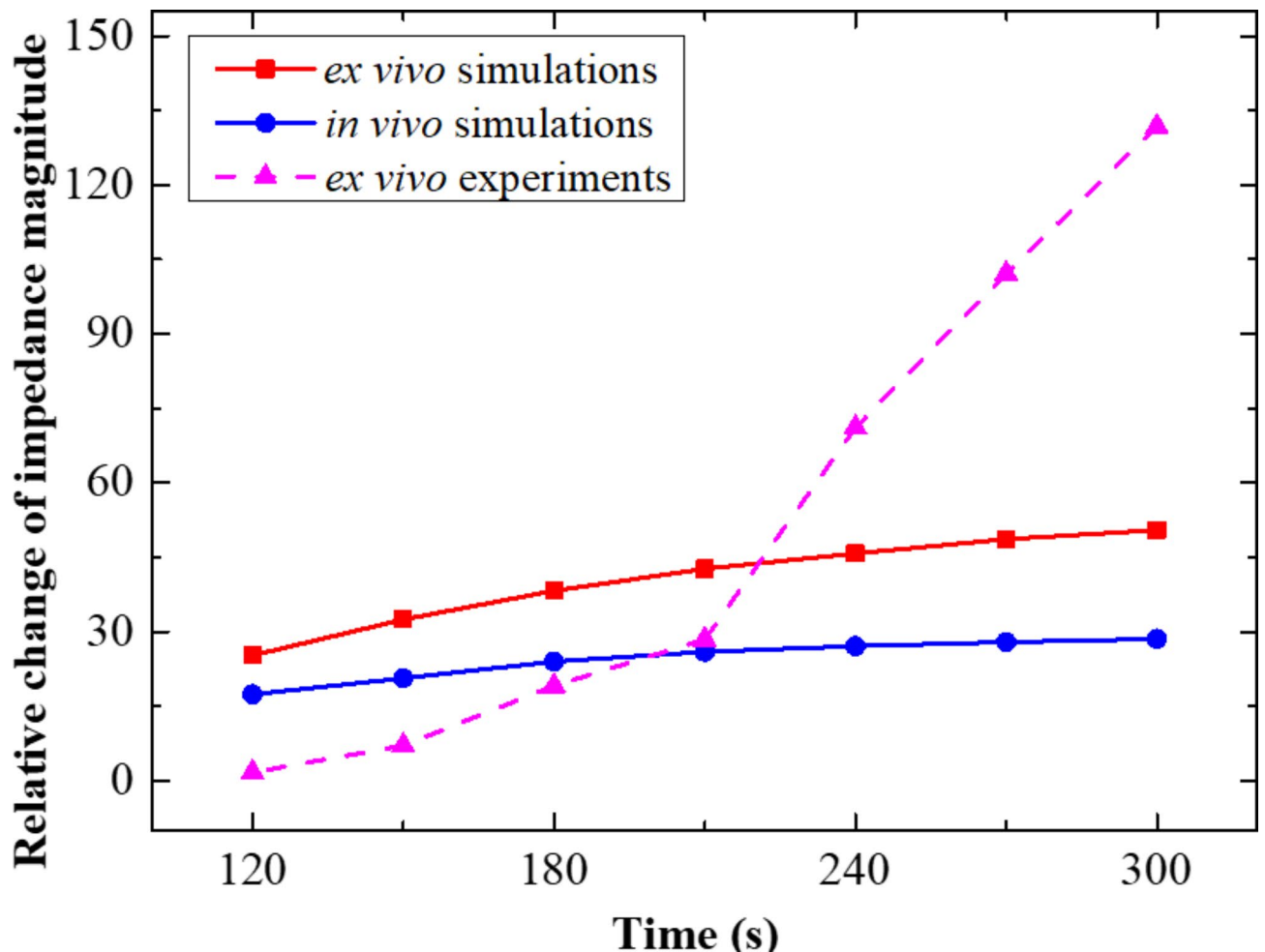
Fig. 9. Comparative results of relative changes in electrical impedance magnitude under simulated and experimental conditions.

was smaller than in the *ex vivo* case, and at the same moment *in vivo* was on average smaller than in *ex vivo* by 18. However, there was no significant difference in their upward trends.

Figure 9 also shows the results of *ex vivo* experimental and computational at 40 W, where the data from the *ex vivo* experiments are taken from Fig. 7a. The relative changes in impedance magnitudes exhibit a consistent upward trend over time. The trend for the simulation results is a slow increase, whereas the *ex vivo* experimental results do increase rapidly. There are some errors in the values, which are due to some ideal conditions set in the simulation parameters. However, this is enough to show that the impedance of porcine liver tissue changes dynamically during the ablation process, which contributes valuable insights into carbonization studies conducted through *ex vivo* experiments.

Conclusion

This paper proposes a method of electrical impedance monitoring for the carbonization of tissues in the ablation center zone. Finite element simulation was used to explore the feasibility of electrical impedance detection during MWA, verifying dynamic changes in the dielectric properties of biological tissues during ablation. The variation in electrical impedance magnitude of *ex vivo* porcine liver tissue during heating was investigated, and carbonization reduction was conducted to regulate the carbonized zone. Real-time monitoring of electrical impedance change magnitude can reduce carbonized tissue formation compared to traditional methods, leading to more precise operations and shorter total ablation times. This method holds significant value for achieving less or no carbonized tumor ablation.

Data availability

The data that support the findings of this study are available upon request from the corresponding author.

References

1. Chu, K. & Dupuy, D. Thermal ablation of tumors: biological mechanisms and advances in therapy. *Nat. Rev. Cancer* **14**, 199–208 (2014).
2. Jin, X. et al. Study on the relationship between reduced scattering coefficient and Young's modulus of tumors in microwave ablation. *Minim. Invasive Ther. Allied Technol.* **30**, 347–355 (2021).
3. Li, G., An, C., Yu, J. & Huang, Q. H. Radiomics analysis of ultrasonic image predicts sensitive effects of microwave ablation in treatment of patient with benign breast tumors. *Biomed. Signal Process. Control.* **76**, 103722 (2022).
4. Bressem, K. K. et al. Exploring patterns of dynamic size changes of lesions after hepatic microwave ablation in an *in vivo* porcine model. *Sci. Rep.* **10**, 805 (2020).
5. Lopresto, V., Pinto, R. & Cavagnaro, M. Experimental characterisation of the thermal lesion induced by microwave ablation. *Int. J. Hyperth.* **30**(2), 110–118 (2014).
6. Fei, G. et al. Experimental study of destruction to porcine spleen *in vivo* by microwave ablation. *World J. Gastroenterol.* **17**(45), 5014–5020 (2011).
7. Ai, H. M. et al. Temperature distribution analysis of tissue water vaporization during microwave ablation: experiments and simulations. *Int. J. Hyperth.* **28**, 674–685 (2012).
8. Salwa, Y., Edgard, J., Sami, E. T. & Antoine, C. Histological study of induced incisions on rabbits' tongues with three diode lasers with different wavelengths in continuous mode. *Scientifica* 1–8 (2018).
9. Liu, F. et al. Ultrasonography-guided percutaneous microwave ablation for large hepatic cavernous haemangiomas. *Int. J. Hyperth.* **34**, 1061–1066 (2018).
10. Cui, R. et al. Microwave ablation assisted by three-dimensional visualization system as local therapy for relapsed hepatoblastoma: a small pilot study. *Abdom. Radiol.* **44**, 2909–2915 (2019).
11. Vita, E. D. et al. Multipoint temperature monitoring of microwave thermal ablation in bones through fiber bragg grating sensor arrays. *Sensors* **20**, 3200 (2020).
12. Schena, E. et al. Solutions to improve the outcomes of thermal treatments in oncology: multipoint temperature monitoring. *IEEE J. Electromag. RF* **2**, 172–178 (2018).
13. Guo, X., Zhou, J., Du, C. & Wang, X. Optical fiber ultrasound probe for radiofrequency ablation temperature monitoring: in-vitro results. *IEEE Photonics Technol. Lett.* **32**, 689–692 (2020).
14. Ni, Y., Mulier, S., Miao, Y., Michel, L. & Marchal, G. A review of the general aspects of radiofrequency ablation. *Abdom. Imaging.* **30**, 381–400 (2005).
15. Yero, D. D., Gonzalez, F. G., Troyen, D. V. & Vandenbosch, G. Dielectric properties of *ex vivo* porcine liver tissue characterized at frequencies between 5 and 500 kHz when heated at different rates. *IEEE Trans. Biomed. Eng.* **65**, 2560–2568 (2018).
16. Hui, T. et al. Microwave ablation of the liver in a live porcine model: the impact of power, time and total energy on ablation zone size and shape. *Int. J. Hyperth.* **37**, 668–676 (2020).
17. Radosevic, A. et al. Short pulsed microwave ablation: computer modeling and *ex vivo* experiments. *Int. J. Hyperth.* **38**, 409–420 (2021).
18. Bedoya, M., Rio, A. D., Chiang, J. & Brace, C. Microwave ablation energy delivery: influence of power pulsing on ablation results in an *ex vivo* and *in vivo* liver model. *Med. Phys.* **41**, 123301 (2014).
19. Jin, X. et al. Temperature control and intermittent time-set protocol optimization for minimizing tissue carbonization in microwave ablation. *Int. J. Hyperth.* **39**, 868–879 (2022).
20. Granchi, S., Vannacci, E., Breschi, L. & Biagi, E. Advantages of cooled fiber for monitoring laser tissue ablation through temporal and spectral analysis of RF ultrasound signal: a case study. *Ultrasonics* **82**, 49–56 (2018).
21. Amini, M., Hisdal, J. & Kalvøy, H. Applications of bioimpedance measurement techniques in tissue engineering. *J. Electr. Bioimpedance* **9**, 142–158 (2018).
22. Leung, K. W. et al. Micro-electrodes for in situ temperature and bio-impedance measurement. *Nano Select* **2**, 1986–1996 (2021).
23. Zhao, Y. et al. Ablation outcome of irreversible electroporation on potato monitored by impedance spectrum under multi-electrode system. *Biomed. Eng. Online* **17**, 1–13 (2018).
24. Jin, X. et al. Evaluation method of *ex vivo* porcine liver reduced scattering coefficient during microwave ablation based on temperature. *Biomed. Tech. (Berl)* **67**(6), 491–501 (2022).
25. Zhang, X. et al. Simulation study of microwave ablation carbonization regulation based on electrical impedance detection. *The Proceedings of the 18th Annual Conference of the China Electrotechnical Society*, vol. 1165, 641–650 (2024).

26. Kassanos, P. Bioimpedance sensors: a tutorial. *IEEE Sens. J.* **21**, 22190–22219 (2021).
27. Ma, G., Hao, Z., Wu, X. & Wang, X. An optimal electrical impedance tomography drive pattern for human-computer interaction applications. *IEEE Trans. Biomed. Circ. Syst.* **14**, 402–411 (2020).
28. McEwan, A., Cusick, G. & Holder, D. S. A review of errors in multi-frequency EIT instrumentation. *Physiol. Meas.* **28**, S197 (2007).
29. Trujillo, M. & Berjano, E. Review of the mathematical functions used to model the temperature dependence of electrical and thermal conductivities of biological tissue in radiofrequency ablation. *Int. J. Hyperth.* **29**, 590–597 (2013).
30. Trujillo, M., Alba, J. & Berjano, E. Relationship between roll-off occurrence and spatial distribution of dehydrated tissue during RF ablation with cooled electrodes. *Int. J. Hyperth.* **28**, 62–68 (2012).
31. Fonseca, R. D. et al. Parametric evaluation of impedance curve in radiofrequency ablation: a quantitative description of the asymmetry and dynamic variation of impedance in bovine *ex vivo* model. *PLoS One* **16**, e0245145 (2021).
32. Chang, I. A. & Nguyen, U. D. Thermal modeling of lesion growth with radiofrequency ablation devices. *Biomed. Eng. Online.* **3**, 27 (2004).
33. Wu, H., Chen, B. & Peng, B. Effects of intratumoral injection of immunoactivator after microwave ablation on antitumor immunity in a mouse model of hepatocellular carcinoma. *Exp. Ther. Med.* **15**, 1914–1917 (2018).
34. Andreozzi, A., Iasiello, M. & Tucci, C. An overview of mathematical models and modulated-heating protocols for thermal ablation. *Adv. Heat. Transf.* **52**, 489–541 (2020).
35. Nijland, H., Zhu, J., Kwee, T. & Jutte, P. Experiments on physical ablation of long bone using microwave ablation; defining optimal settings using ex-and in-vivo experiments. *PLoS One* **18**, e0284027 (2023).
36. Rhim, H. et al. Essential techniques for successful radio-frequency thermal ablation of malignant hepatic tumors. *Radiographics* **21**, S17–S35 (2001).
37. Liu, K. & Chen, T. M. Comparative study of heat transfer and thermal damage assessment models for hyperthermia treatment. *J. Therm. Biol.* **98**, 102907 (2021).
38. Jones, C., Badger, S. A. & Ellis, G. The role of microwave ablation in the management of hepatic colorectal metastases. *Surg. J. R. Coll. Serg E* **9**(1), 33–37 (2011).
39. Hall, S. K., Ooi, E. H. & Payne, S. J. Cell death, perfusion and electrical parameters are critical in models of hepatic radiofrequency ablation. *Int. J. Hyperth.* **31**(5), 538–550 (2015).

Acknowledgements

Author contributions

Z. X., W. W., X. L., and J. X. were responsible for the ablation performance, conceptualization and methodology, and for the bioelectrical impedance system setup. Z. X. and Q. L. contributed to the MWA system and data analysis. Y. L. produced high-quality charts and graphs. X. L., J. X., and Q. Z. contributed to the review of the work critically for important intellectual content and final approval of the version to be published. All authors reviewed the manuscript.

Declarations

Competing interests

The authors declare no competing interests.

Additional information

None of the experiments were performed on in vivo animals. All ex vivo porcine liver was chosen as the material for the experiment. Fresh ex vivo porcine liver was obtained from the local slaughterhouse and used the same day.

Additional information

Correspondence and requests for materials should be addressed to X.J. or L.X.

Reprints and permissions information is available at www.nature.com/reprints.

Publisher's note Springer Nature remains neutral with regard to jurisdictional claims in published maps and institutional affiliations.